Schizophrenia Bulletin vol. 41 no. 5 pp. 1123–1132, 2015
doi:10.1093/schbul/sbv030
Advance Access publication March 27, 2015

Elevated Excitatory Input to the Nucleus Accumbens in Schizophrenia: A Postmortem Ultrastructural Study

Lesley A. McCollum*[,1], Courtney K. Walker[2], Joy K. Roche[1], and Rosalinda C. Roberts[1]

[1]Department of Psychiatry and Behavioral Neurobiology, University of Alabama at Birmingham, Birmingham, AL; [2]Department of Psychology, University of Alabama at Birmingham, Birmingham, AL

*To whom correspondence should be addressed; Department of Psychiatry and Behavioral Neurobiology, University of Alabama at Birmingham, Sparks Center 841, 1720 2nd Avenue South, Birmingham, AL 35294, US; tel: +1-205-934-1858, fax: +1-205-996-9377, e-mail: lbryant@uab.edu

The cause of schizophrenia (SZ) is unknown and no single region of the brain can be pinpointed as an area of primary pathology. Rather, SZ results from dysfunction of multiple neurotransmitter systems and miswiring between brain regions. It is necessary to elucidate how communication between regions is disrupted to advance our understanding of SZ pathology. The nucleus accumbens (NAcc) is a prime region of interest, where inputs from numerous brain areas altered in SZ are integrated. Aberrant signaling in the NAcc is hypothesized to cause symptoms of SZ, but it is unknown if these abnormalities are actually present. Electron microscopy was used to study the morphology of synaptic connections in SZ. The NAcc core and shell of 6 SZ subjects and 8 matched controls were compared in this pilot study. SZ subjects had a 19% increase in the density of asymmetric axospinous synapses (characteristic of excitatory inputs) in the core, but not the shell. Both groups had similar densities of symmetric synapses (characteristic of inhibitory inputs). The postsynaptic densities of asymmetric synapses had 22% smaller areas in the core, but not the shell. These results indicate that the core receives increased excitatory input in SZ, potentially leading to dysfunctional dopamine neurotransmission and cortico-striatal-thalamic stimulus processing. The reduced postsynaptic density size of asymmetric synapses suggests impaired signaling at these synapses. These findings enhance our understanding of the role the NAcc might play in SZ and the interaction of glutamatergic and dopaminergic abnormalities in SZ.

Key words: electron microscopy/anatomy/striatum/synapse

The exact pathophysiology for the origin of schizophrenia (SZ) is unknown, however evidence from decades of research implies that interactions between multiple brain regions and multiple neurotransmitter systems are likely at play. One region that is implicated in SZ pathology is the nucleus accumbens (NAcc). The NAcc integrates signaling from multiple regions of the brain, receiving input from areas including the prefrontal cortex, hippocampus, amygdala, thalamus, and midbrain.[1] Importantly, all of these areas have been associated with SZ, making the NAcc a prime region for integrating multiple disrupted areas to provide a comprehensive understanding of SZ pathology.[2] Reciprocal connections between the NAcc and substantia nigra/ventral tegmental area (SN/VTA) indicate further importance of this region. Via these connections, the NAcc modulates dopaminergic input to the dorsal striatum,[3] and striatal dopamine (DA) dysfunction is a hallmark characteristic of the disorder.[4] Though many studies have implicated the NAcc in SZ, none have been able to describe its circuitry.

The purpose of this study was to provide the first ultrastructural analysis in postmortem human NAcc, and examine the neurocircuitry in the NAcc in SZ to establish the role this region may play in the disorder. We used stereological analysis of electron micrographs in postmortem SZ to analyze the organization and composition of synapse types in the NAcc.

Methods

Brain Tissue

Postmortem human tissue was obtained from the Alabama and Maryland Brain Collections, with consent from the next of kin. The tissue was collected from 8 control and 6 SZ subjects. Cases were diagnosed based on patient medical records, family interviews, autopsy reports, and neuropathologic assessments. DSM-IV diagnosis of SZ was confirmed independently by two psychiatrists. All SZ cases except one were on antipsychotic drugs (APD) at the time of death. Control cases had no history of psychiatric or neurological disease.

Pairs of control and SZ cases were chosen based on the best match of age, race, sex, postmortem interval (PMI), and tissue pH level. Some of the control (n = 3) and SZ (n = 5) cases used in this study have also been used in previous studies analyzing synaptic density of the dorsal striatum.[5–9] Coronal blocks of the striatum were immersed in 4% paraformaldehyde and 1% glutaraldehyde in 0.1 M phosphate buffer for at least 1 week (4°C). Striatal tissue was then sectioned at a thickness of 40 µm with a Vibratome into 6 free-floating series.

Core/Shell Mask

To visualize subregions of the NAcc, 1 series from each case was processed for immunolabeling of calbindin. This series was then used to create a mask of the NAcc core and shell boundary for use when blocking tissue for electron microscopy (figure 1A).

The primary antibody was mouse monoclonal anti-calbindin (Sigma, C9848; 1:1000). The secondary antibody was biotinylated horse anti-mouse IgG (Vector Laboratories; 1:400). Antibodies were prepared in 3% normal horse serum in phosphate buffered saline containing 0.3% triton X-100. The tissue was pretreated in citrate buffer for 30 min in an 80°C water bath for antigen retrieval. The immunohistochemistry protocol was performed as detailed previously.[10]

Electron Microscopy

A second series was flat embedded for electron microscopic analysis using standard techniques, as detailed previously.[10] Regions from the core and shell were blocked using the calbindin-stained sections as a guide. For each region, 3 blocks per case, at least 240 µm apart rostrocaudally, were used to obtain semithin sections.

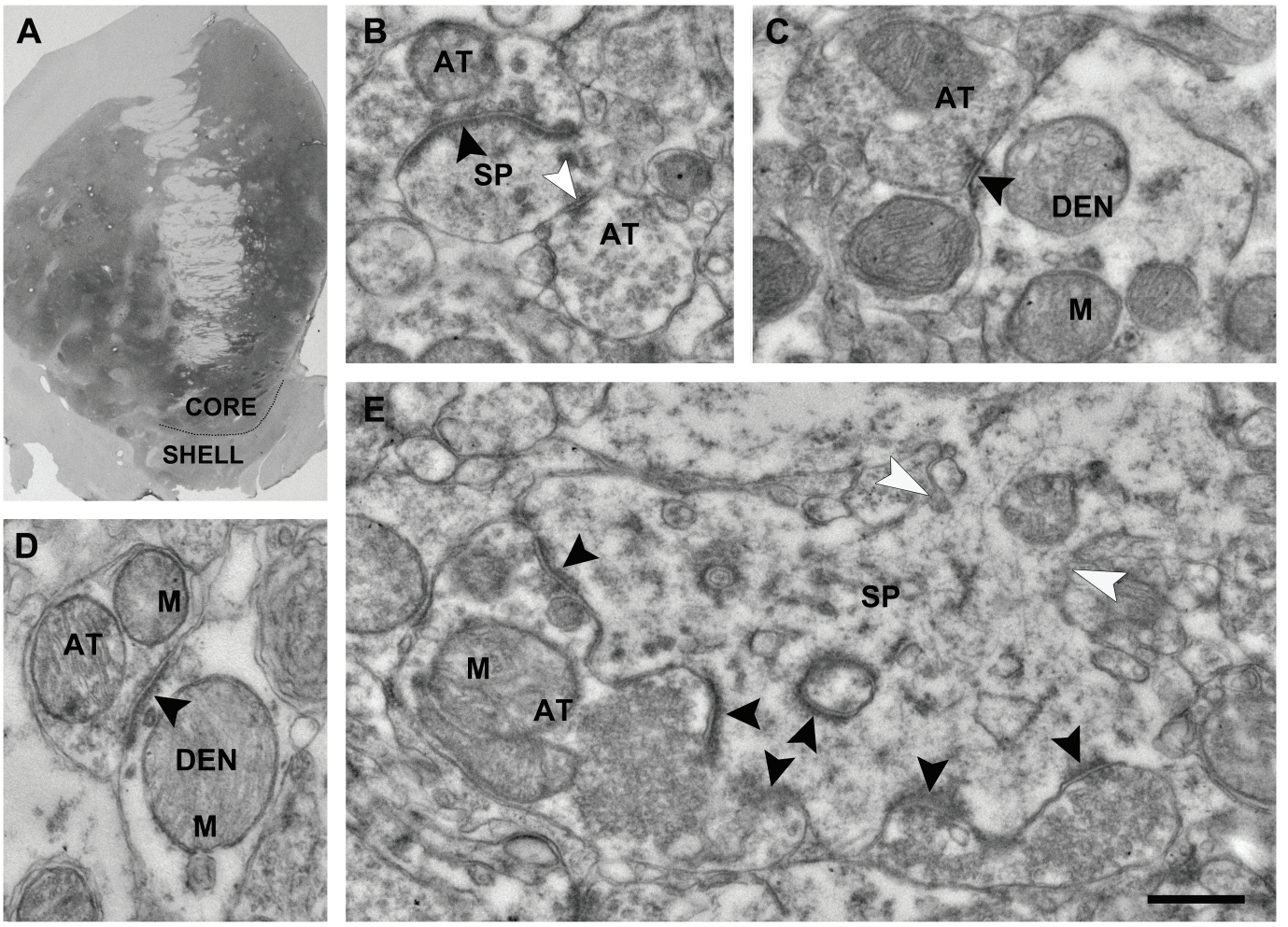

Fig. 1. Ultrastructure of the human NAcc. (A) A representative calbindin-stained section used as a mask for the core/shell boundary. Blocks from each region were then taken from an adjacent embedded section for EM. (B) A spine (SP) receives convergent input from axon terminals (AT) making asymmetric (black arrowhead) and symmetric (white arrowhead) synapses. (C) An AT forms a symmetric synapse (arrowhead) with a dendrite (DEN). (D) An AT forms an asymmetric synapse (arrowhead) with a DEN. (E) An AT forms an elaborate multi-perforated synapse with a SP. The SP was observed through multiple serial sections and synaptic contact was made at each of the arrowheads. The neck of the SP is marked by the white arrows. M, mitochondrion. Scale bar (B–E) = 500 nm.

These sections (250 nm thickness) were collected using an ultramicrotome, mounted on glass slides, stained with Toluidine Blue and coverslipped for reference. Serial ultrathin sections (90 nm thickness) from each block were mounted on Formvar-coated copper grids, and photographed at 80 kV on a Hitachi transmission electron microscope, as detailed previously.[10]

Data collection and statistical analyses

To determine the number of synapses in the neuropil, serial sections were analyzed using the disector technique.[11,12] An average of seven consecutive sections per block were used as disector reference sections, yielding a combined total of 540 sections analyzed for this study. The average sampling volume was 294 μm^3 per block. All synapses in this study were identified by the first and last authors. Micrographs were cropped and adjusted for brightness and contrast for presentation in the figures. Criteria for distinguishing a synapse were the presence of (1) parallel pre- and postsynaptic membranes, (2) a postsynaptic density (PSD), and (3) synaptic vesicles at the membrane in the presynaptic terminal. Synaptic features quantified using stereology included the symmetry of the PSD and the postsynaptic target. Neuropil only was quantified, cell bodies were not photographed. Using stereology, an average of 176 ± 34 synapses were counted in 869.5 ± 55.7 μm^3 of the core, and 160 ± 30 synapses in 844.8 ± 104.9 μm^3 of the shell, per case. This yielded a total of 2459 synapses in 12173.5 μm^3 of the core, and 2076 synapses in 10982.2 μm^3 of the shell.

Additionally, serial images were used to quantify PSD and mitochondrial measurements. For PSD measurements, 2 sets of 8 serial electron micrographs per region per case were analyzed resulting in approximately 60 synapses measured per case. The length along the postsynaptic membrane and outline of the PSD were traced by hand using NIH ImageJ. Average thickness was calculated by dividing the area of the PSD by the measured length.[13] Mitochondria were analyzed in 1 micrograph per region per case, yielding an average of 296 mitochondria analyzed per case. Mitochondria were counted and normalized to an area of 1000 μm^2. Their diameters were measured along the short axis using ImageJ. Calcium deposits within mitochondria were counted. For PSD and mitochondrial measurements, serial images were used to verify that measurements were taken from a full cross-section of the synapse.

Striatal area was measured in the adjacent, calbindin-stained sections in ImageJ. The full outlines of the striatal sections were traced and area was measured in cm^2. Cases in which the complete striatum was not available were excluded from this analysis, resulting in a final sample size for striatal area of $n = 4$ and $n = 5$ for control and SZ groups, respectively.

For all analyses, core and shell were analyzed separately. Data from all cases within a group were averaged for each region and statistical tests were performed on average values. All data sets were assessed for normality with the Kolmogorov–Smirnov test, then the corresponding parametric (*t*-test) or nonparametric (Wilcoxon) tests were performed for group comparisons. All statistical tests were 2-tailed with significance of $P < 0.05$.

Results

The control and SZ groups were well matched for age, race, gender, PMI, and pH (table 1). The quality of ultrastructural preservation in control and SZ cases was similar and no obvious morphological pathology was present in the SZ cases. The core and shell subregions within each group were qualitatively similar. Asymmetric axospinous (AS) synapses were most frequently observed in both regions of the groups, though symmetric axospinous (SS), asymmetric axodendritic (AD), and symmetric axodendritic (SD) were also observed (figures 1B–D). Very few (<1%) synapses that met all of the criteria listed above were too ambiguous to be classified as a specific synapse type. Some spines received convergent asymmetric and symmetric input from two distinct terminals (figure 1B). Large elaborate synapses with multiple perforations made up 4% of synapses in the core and 2.5% in the shell (figure 1E). Their densities were consistent between groups in both regions, as were other characteristics such as PSD length, area, and number of perforations. There was no difference in the area of the entire striatum between groups (control: 3.72 ± 0.64 cm^2, SZ: 3.58 ± 0.64 cm^2, $P = 0.76$).

Synapse Types

Within the core, there was an increased density of total synapses in the SZ group (figure 2A); 0.18 ± 0.01 per μm^3 in control compared to 0.22 ± 0.04 per μm^3 in SZ ($P = 0.04$). This increased density was found only in asymmetric synapses; symmetric synapses had a similar density between the 2 groups. Further, when analyzing synapse subtypes, the increased density was found

Table 1. Case Demographics

	CTRL	SZ
n	8	6
Age, years	52.3 ± 19.8	52.0 ± 12.5
Race	3AA, 5C	1AA, 5C
Gender	4M, 4F	3M, 3F
PMI, h	6.9 ± 1.4	5.4 ± 1.8
pH	6.8 ± 0.3	6.8 ± 0.4

Note: Mean ± SD. PMI, postmortem interval; AA, African American; C, Caucasian; M, male; F, female; CTRL, control; SZ, schizophrenia.

exclusively in AS synapses (figure 2B); 0.13 ± 0.01 per μm³ in control compared to 0.16 ± 0.03 per μm³ in SZ (P = 0.04). The density of all axospinous synapses was increased at a trend level (P = 0.054). These differences were unique to the core region; the shell had similar densities of all synapse types between the 2 groups (figures 2A and 2B). Although the density of only one synapse type was significantly increased in SZ, there was a trend for an increase in all types in the core (figure 2C).

Postsynaptic Density

Analysis of PSDs revealed a significant reduction in PSD area in both the core and shell (figure 3B). In the synapse subtypes of the core, there was a significant reduction in PSD area of AS synapses (figure 3C), and in PSD thickness of AD synapses (thickness data not shown). Analysis of individual subtypes in the shell revealed no significant differences in the control and SZ groups (figure 3C). These differences were unique to asymmetric synapses;

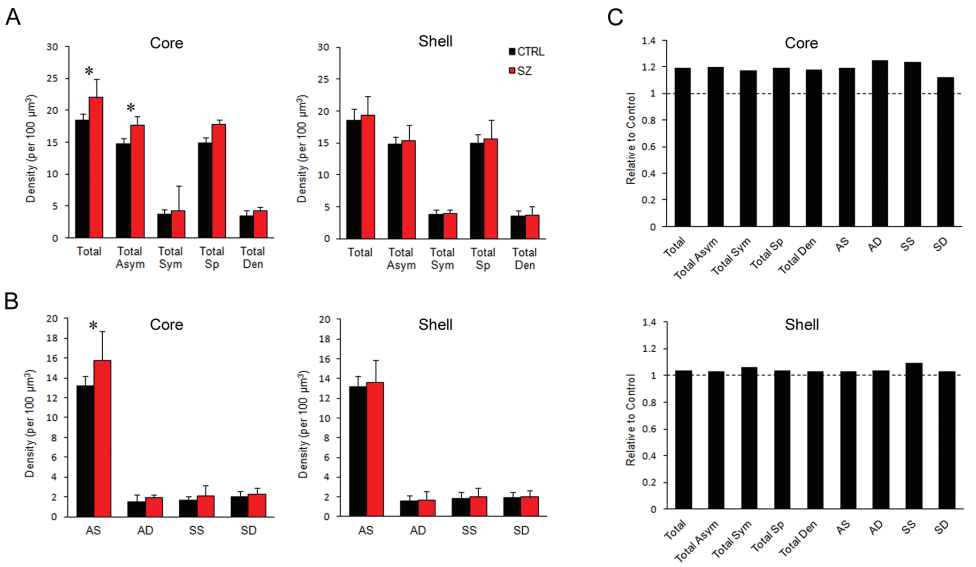

Fig. 2. Synaptic density in the core and shell. (A) Density of all synapses (Total), and grouped by symmetry of PSD: all asymmetric (Total Asym) and symmetric (Total Sym) synapses, or by postsynaptic target: all axospinous (Total Sp) and axodendritic (Total Den) synapses. (B) Density of synapse types: asymmetric axospinous (AS), asymmetric axodendritic (AD), symmetric axospinous (SS), and symmetric axodendritic (SD). (**C**) Synapse density relative to control. The dotted line represents the control level. *P < .05.

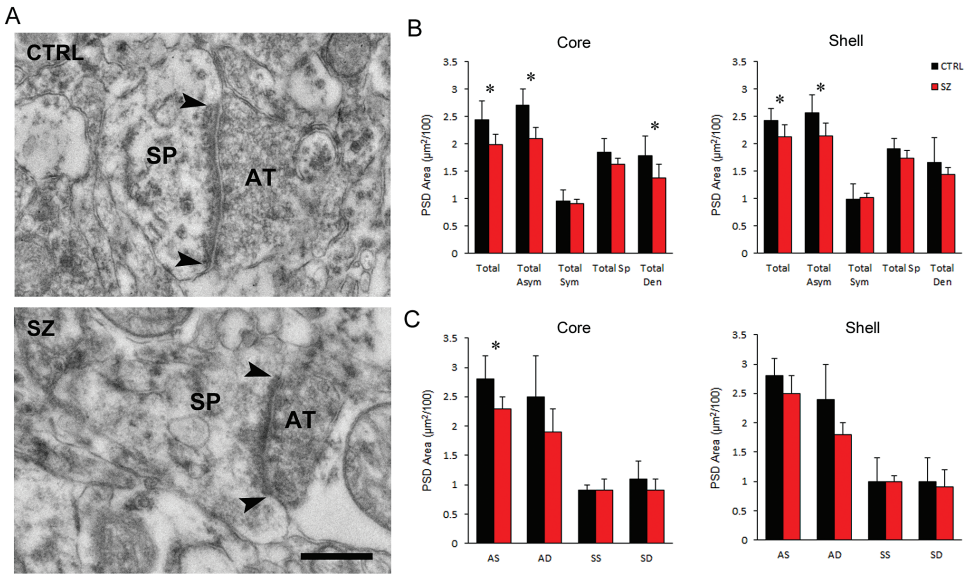

Fig. 3. Area of the PSD in the core and shell. (A) Example AS synapses from control (CTRL) and SZ electron micrographs that were analyzed for PSD size. Scale bar = 500 nm. (B) PSD area of all synapses (Total), and grouped by symmetry of PSD: all asymmetric (Total Asym) and symmetric (Total Sym) synapses; or by postsynaptic target: all axospinous (Total Sp) and axodendritic (Total Den) synapses. (C) PSD area of each synapse type: asymmetric axospinous (AS), asymmetric axodendritic (AD), symmetric axospinous (SS), and symmetric axodendritic (SD). *P < .05.

symmetric synapses had similar PSD size between groups in both the core and shell.

Mitochondria

The qualitative health and general appearance of the mitochondria were normal in both groups. Quantification of the number of mitochondria in the neuropil (per 1000 μm^2) and their average diameter was similar for both groups in the core and shell (table 2). Similarly, the number of calcium deposits per mitochondrion in SZ was similar to that in controls in both regions (table 2).

Discussion

This study is the first to examine the neurocircuitry of the NAcc in healthy or diseased postmortem human tissue at the electron microscopic level. Our findings in the SZ subjects suggest an increase in glutamatergic-type input and a similar density of dopaminergic-type input in SZ. The differences identified at the ultrastructural level indicate abnormal wiring in the circuitry of the NAcc in SZ which could be contributing to the pathophysiology of the disease.

Overview of Human NAcc Ultrastructure

The ultrastructure of the human NAcc was similar to that described in nonhuman primates and rodents.[14–19] The elaborate multi-perforated synapses, however, have not been reported in other species or in other regions of the human brain. Increased spine volume, synapse length, and perforations are all associated with increased synaptic activity.[20–22] Thus, these synapses could be a manifestation of the complex interconnectivity of the NAcc with many other brain regions. Since they were present in both groups they seem to be a unique characteristic of the human NAcc, independent of the disease state.

Elevated Excitatory Input in SZ

The increase in AS synapses indicates an increase in glutamatergic-type input to the region. This is consistent with findings in the dorsal striatum which also found an increase in AS synapses in SZ.[6] In agreement with this finding is evidence for an increased expression of the excitatory PSD protein SAP90/PSD-95-associated protein 1 (SAPAP1) in the NAcc in postmortem SZ.[23] Rodent models of SZ also exhibit increased indices of glutamatergic-type input in the NAcc; rats treated with psychotomimetics have increased mRNA expression of excitatory PSD genes,[23,24] and increased dendritic spine density in the NAcc,[25–27] which is tightly correlated with the density of AS synapses.[28] A likely source of this elevated input in SZ and its functional implications are discussed below.

Table 2. Mitochondrion Quantifications

	CTRL	SZ
Core		
Total (per 1000 μm^2)	312 ± 40	302 ± 90
Diameter (μm)	0.46 ± 0.02	0.45 ± 0.04
Calcium deposits[a] (*n*)	0.44 ± 0.15	0.57 ± 0.13
Shell		
Total (per 1000 μm^2)	333 ± 46	293 ± 56
Diameter (μm)	0.44 ± 0.01	0.45 ± 0.04
Calcium deposits[a] (*n*)	0.49 ± 0.14	0.46 ± 0.17

Mean ± SD. CTRL, control; SZ, schizophrenia.
[a]Per mitochondrion.

Reduced PSD Size

Our findings indicate a reduction in the PSD size of excitatory synapses in SZ. The PSD consists of many different proteins for scaffolding and signaling at the synapse.[29] The size and composition of PSDs are dynamic, changing with activity of the synapse[13,30,31] and are proportional to the area of the spine head.[32–35]

A reduction in the size of asymmetric PSDs could indicate abnormalities in membrane receptors or signaling molecules of glutamatergic synapses. Several studies have investigated glutamatergic receptors in the NAcc in SZ, and have consistently found no difference in mGluR,[36,37] NMDA,[36,38,39] AMPA,[36,39–41] or kainate[36,39] receptor expression and binding. Thus, it is unlikely that the reduced PSD size found in this study is due to a reduction in glutamate receptor expression. Very few studies have investigated signaling molecules of glutamatergic synapses in the NAcc,[23,42] and do not report conclusive findings to explain the reduced PSD size found in the present study.

It is possible that the reduced PSD size is a consequence of overstimulation from the excessive glutamatergic afferents also found in this study. If elevated glutamatergic input to the NAcc is indeed involved in the pathophysiology of SZ, it is possible that this excessive excitation could result in the degeneration or reorganization of synaptic structure over time. While no morphological signs were observed in the tissue that indicated excitotoxic degeneration, many PSD proteins are involved in the mechanism of excitotoxicity,[43] and this could provide an explanation for the reduced PSD size at excitatory synapses reported here.

Similar Inhibitory Input in SZ

A similar density of symmetric synapses (axodendritic and axospinous) was found in the control and SZ groups. Within the striatum, symmetric synapses are formed by interneurons and dopaminergic projections from the SN/VTA. DA inputs form symmetric synapses on both dendrites and spines.[15,44] Thus, the similar density of these synapses suggests that the NAcc does not have increased inhibitory input from intrinsic interneurons, nor does it receive increased dopaminergic input from the SN/VTA

in SZ. While this suggests that dopaminergic input to the region is normal in SZ, it remains possible that DA is being abnormally produced in the same number of axon terminals, or that abnormal modulation by glutamatergic afferents could result in the dysregulation of its release, as discussed below.

Similar Morphological State of Mitochondria

The structural integrity of the mitochondria in the NAcc does not indicate drastic abnormalities in metabolic demand of the region in SZ. This finding contrasts previous ultrastructural studies in the dorsal striatum which found differences in the number and distribution of mitochondria in SZ subjects compared to controls.[45–48] Few studies have considered the structure and function of mitochondria in the NAcc in SZ.[49–52] Differential alterations in the basal ganglia have been reported in SZ, including increased mitochondrial activity in the NAcc of paranoid SZ subjects that was attributed to APD effects.[51] Despite the evidence for mitochondrial pathology in dorsal striatum in SZ, our structural findings do not indicate this pathology is present in the NAcc.

Differences in NAcc Core and Shell

An interesting finding to emerge in this study was that group differences were primarily found in the core. The shell of control and SZ subjects was similar across nearly all measures. The afferent and efferent connections of the core and shell regions have been identified in rats and nonhuman primates.[1,53,54] While many of the connections overlap, there are distinct differences that lead to different functional roles of the 2 subregions.[1,55] Studies in animal models have found the regions respond differently to APD, and have often concluded that the shell must play a larger role in SZ due to the strength of APD action here compared to the core.[56–58] It is interesting then that our findings are sequestered to the core. The afferent and efferent connections of the core parallel those of the dorsal striatum, while the shell has been considered a transition zone between the striatum and the extended amygdala.[59–61] Thus, our findings localized to the core further support the redefined hypothesis for the role of the associative striatum, rather than the limbic striatum, in SZ.[62]

Evaluating the Role of the NAcc in SZ

The NAcc has long been implicated in the etiology of SZ, and is often assumed to be the locus of elevated striatal DA characteristic of SZ. This assumption was typically founded on evidence for antipsychotic action in the NAcc,[56–58,63] as well as its functional role in the brain which provided a logical link between the pathology and symptomatology of SZ. Recent imaging studies, however, have found the associative striatum, not the limbic striatum, to be the locus of elevated striatal DA.[64,65] The morphological findings in postmortem tissue from the present study support the imaging findings by suggesting that the NAcc does not receive elevated dopaminergic input.

While this is an interesting development in understanding the critical role that striatal DA plays in both the pathology and treatment of SZ, it does not exclude the NAcc from the equation of SZ etiology. The evidence for elevated glutamatergic-type input to the NAcc in the present study indicates abnormal signaling in the region. The findings reported here are highly consistent with the hypothesis for excessive glutamatergic input to the NAcc driving symptoms of SZ.[2,66–69]

The NAcc receives glutamatergic input from the cortex, thalamus, hippocampus, and amygdala. Afferent connections from each of these regions have similar ultrastructural morphology in the NAcc, typically forming AS synapses.[70] Thus, the elevated input seen in SZ could be arising from any of these regions. A possible source for the increased input is the hippocampus. There is evidence for a reduction in GABAergic interneurons in the hippocampus in SZ[71–74] as well as an increase in hippocampal activity at rest.[75,76] In this context, one might expect to see elevated input in the shell rather than the core since the shell receives denser hippocampal input than the core. However, anterograde tracing studies show that the hippocampus projects to all of the NAcc in a topographical manner,[77,78] so it is possible that the increased input results from abnormalities of a specific hippocampal subregion projecting to the core.

Excessive excitatory input to the NAcc would result in significant consequences for the flow of information through this region. DA is released in the NAcc upon stimulation of the ventral subiculum of the hippocampus,[79–81] and increased activity in the ventral hippocampus drives DA dysfunction in an animal model of SZ.[69] Further, glutamatergic input from the hippocampus and amygdala provide a gating mechanism for information flow through the NAcc; input from either of these regions is required for signals from the prefrontal cortex to continue its flow through the cortico-striato-thalamic loop.[82] Thus, elevated glutamatergic input to the NAcc could result in increased dopaminergic release and/or a hyperresponsive system.[2]

These hypotheses implicate glutamatergic dysregulation of NAcc in positive symptoms of SZ, however it is also well established that the NAcc is involved in reward and motivation, the loss of which constitute some of the negative symptoms of SZ. It has been hypothesized that a loss of gating in the NAcc, possibly due to elevated glutamatergic input and subsequent DA dysregulation, could result in increased signal noise in the region; this would effectively diminish the response to stimuli otherwise eliciting reward or motivated behavior.[83,84] The elevated glutamatergic-type input and similar density of

dopaminergic-type input provide the first structural data in the NAcc of SZ subjects to support the hypothesis that excessive hippocampal input to the NAcc could be a pathological mechanism of SZ.[2,66–69]

Limitations

While the functional consequences of these structural findings can only be speculated, this study provides vital insight for understanding the structural pathology that leads to symptoms in SZ. Forming a link between pathology of the neurocircuitry in SZ and the functional outcomes will be a powerful tool for moving forward in our understanding of the cause, as well as improving treatment for SZ.

The small sample size should be taken into consideration with the interpretation of these findings. With the heterogeneity of SZ, it is likely that the cohort analyzed for this study does not represent all aspects of the disorder. However, the results agree with studies of synaptic density in the dorsal striatum in SZ[6] and are consistent with hypotheses of SZ. Postmortem SZ subjects suitable for electron microscopy are rare, so the cohort collected for this study, although small, provides a unique analysis of postmortem SZ.

All but one of the subjects in the present study were chronically medicated at the time of death, thus it is possible that our results are due to APD treatment. Ultrastructural studies of APD effects in the striatum primarily focus on the dorsal striatum, where chronic (6 months or longer) haloperidol treatment results in reduced asymmetric synapse density[85,86] and reduced spine number.[87] Other studies of APD treatment have reported an increased percentage of perforated synapses in the caudate with no change in total number, and no differences present in the NAcc.[88–90] These studies do not indicate our results are due to APD treatment. Past studies also indicate that APDs increase striatal volume;[91–95] thus, our finding of increased AS synaptic density is likely not an effect of medication, since a larger volume would reduce synaptic density rather than increase it. Rather, it is possible that an increased striatal volume in SZ subjects could result in false negatives or dampen measured increases in density in our study.

Stereological studies provide the advantage of estimating total object number and thus avoiding volume discrepancies. The estimation of total number, however, requires distinct regional boundaries, and it is well established that no distinct boundary exists between the NAcc core and ventral caudate/putamen regions.[54,60,96–98] Thus, an analysis of total object number would have required introducing arbitrary and nonreplicable region boundaries due to the variability between human brains. This issue was addressed by using unbiased stereology to measure object density paired with measuring striatal volume. The striatal volumes did not significantly differ between the two groups which further confirms that our findings are not due to volume differences.

Conclusions

This study provides not only the first ultrastructural quantitative analysis performed in human NAcc, but also an analysis of the NAcc ultrastructure in SZ. Our findings indicate miswiring of the neurocircuitry in the NAcc core in SZ, specifically an increase in glutamatergic-type input. We argue that this is unique to the etiology of the disorder and may provide a morphological link between glutamatergic pathology and striatal DA pathology in SZ.

Funding

National Institute of Mental Health (F31MH098566 to L.A.M. and RO1MH066123 to R.C.R.).

Acknowledgments

The authors would like to thank the staff of the Alabama Brain Collection and Maryland Brain Collection for the samples used in this study.

References

1. Groenewegen HJ, Trimble M. The ventral striatum as an interface between the limbic and motor systems. *CNS Spectr*. 2007;12:887–892.
2. Grace AA. Gating of information flow within the limbic system and the pathophysiology of schizophrenia. *Brain Res Brain Res Rev*. 2000;31:330–341.
3. Haber SN, Fudge JL, McFarland NR. Striatonigrostriatal pathways in primates form an ascending spiral from the shell to the dorsolateral striatum. *J Neurosci*. 2000;20:2369–2382.
4. Miyake N, Thompson J, Skinbjerg M, Abi-Dargham A. Presynaptic dopamine in schizophrenia. *CNS Neurosci Ther*. 2011;17:104–109.
5. Kung L, Conley R, Chute DJ, Smialek J, Roberts RC. Synaptic changes in the striatum of schizophrenic cases: a controlled postmortem ultrastructural study. *Synapse*. 1998;28:125–139.
6. Roberts RC, Roche JK, Conley RR. Synaptic differences in the postmortem striatum of subjects with schizophrenia: a stereological ultrastructural analysis. *Synapse*. 2005;56:185–197.
7. Roberts R, Roche J, Conley R. Synaptic differences in the patch matrix compartments of subjects with schizophrenia: a postmortem ultrastructural study of the striatum. *Neurobiol Dis*. 2005;20:324–335.
8. Roberts RC, Roche JK, Conley RR. Differential synaptic changes in the striatum of subjects with undifferentiated versus paranoid schizophrenia. *Synapse*. 2008;62:616–627.
9. Roberts RC, Roche JK, Conley RR, Lahti AC. Dopaminergic synapses in the caudate of subjects with schizophrenia: relationship to treatment response. *Synapse*. 2009;63:520–530.
10. McCollum LA, Roberts RC. Ultrastructural localization of tyrosine hydroxylase in tree shrew nucleus accumbens core and shell. *Neuroscience*. 2014;271:23–34.

11. Sterio DC. The unbiased estimation of number and sizes of arbitrary particles using the disector. *J Microsc*. 1984;134:127–136.
12. Perez-Costas E, Melendez-Ferro M, Roberts RC. Microscopy techniques and the study of synapses. In: Mendez-Vilas A, Diaz J, eds. *Modern Research and Educational Topics in Microscopy*. 3rd ed. Badajoz, Spain: Formatex; 2007:164–170.
13. Dosemeci A, Tao-Cheng J-H, Vinade L, Winters C, Pozzo-Miller L, Reese T. Glutamate-induced transient modification of the postsynaptic density. *Proc Natl Acad Sci*. 2001;98:10428–10432.
14. Arluison M, Dietl M, Thibault J. Ultrastructural morphology of dopaminergic nerve terminals and synapses in the striatum of the rat using tyrosine hydroxylase immunocytochemistry: a topographical study. *Brain Res Bull*. 1984;13:269–285.
15. Bouyer JJ, Joh TH, Pickel VM. Ultrastructural localization of tyrosine hydroxylase in rat nucleus accumbens. *J Comp Neurol*. 1984;227:92–103.
16. Voorn P, Jorritsma-Byham B, Van Dijk C, Buijs RM. The dopaminergic innervation of the ventral striatum in the rat: a light- and electron-microscopical study with antibodies against dopamine. *J Comp Neurol*. 1986;251:84–99.
17. Zahm DS. An electron microscopic morphometric comparison of tyrosine hydroxylase immunoreactive innervation in the neostriatum and the nucleus accumbens core and shell. *Brain Res*. 1992;575:341–346.
18. Ikemoto K, Satoh K, Kitahama K, Geffard M, Maeda T. Electron-microscopic study of dopaminergic structures in the medial subdivision of the monkey nucleus accumbens. *Exp Brain Res*. 1996;111:41–50.
19. Bérubé-Carrière N, Guay G, Fortin G, et al. Ultrastructural characterization of the mesostriatal dopamine innervation in mice, including two mouse lines of conditional VGLUT2 knockout in dopamine neurons. *Eur J Neurosci*. 2012;35:527–538.
20. Calverley RK, Jones DG. Contributions of dendritic spines and perforated synapses to synaptic plasticity. *Brain Res Brain Res Rev*. 1990;15:215–249.
21. Hering H, Sheng M. Dendritic spines: structure, dynamics and regulation. *Nat Rev Neurosci*. 2001;2:880–888.
22. Yuste R, Bonhoeffer T. Morphological changes in dendritic spines associated with long-term synaptic plasticity. *Annu Rev Neurosci*. 2001;24:1071–1089.
23. Kajimoto Y, Shirakawa O, Lin XH, et al. Synapse-associated protein 90/postsynaptic density-95-associated protein (SAPAP) is expressed differentially in phencyclidine-treated rats and is increased in the nucleus accumbens of patients with schizophrenia. *Neuropsychopharmacology*. 2003;28:1831–1839.
24. Iasevoli F, Polese D, Ambesi-Impiombato A, Muscettola G, de Bartolomeis A. Ketamine-related expression of glutamatergic postsynaptic density genes: possible implications in psychosis. *Neurosci Lett*. 2007;416:1–5.
25. Robinson TE, Kolb B. Persistent structural modifications in nucleus accumbens and prefrontal cortex neurons produced by previous experience with amphetamine. *J Neurosci*. 1997;17:8491–8497.
26. Robinson TE, Kolb B. Alterations in the morphology of dendrites and dendritic spines in the nucleus accumbens and prefrontal cortex following repeated treatment with amphetamine or cocaine. *Eur J Neurosci*. 1999;11:1598–1604.
27. Flores C, Wen X, Labelle-Dumais C, Kolb B. Chronic phencyclidine treatment increases dendritic spine density in prefrontal cortex and nucleus accumbens neurons. *Synapse*. 2007;61:978–984.
28. Harris KM, Kater SB. Dendritic spines: cellular specializations imparting both stability and flexibility to synaptic function. *Annu Rev Neurosci*. 1994;17:341–371.
29. Sheng M, Hoogenraad CC. The postsynaptic architecture of excitatory synapses: a more quantitative view. *Annu Rev Biochem*. 2007;76:823–847.
30. Bosch M, Castro J, Saneyoshi T, Matsuno H, Sur M, Hayashi Y. Structural and molecular remodeling of dendritic spine substructures during long-term potentiation. *Neuron*. 2014;82:444–459.
31. Meyer D, Bonhoeffer T, Scheuss V. Balance and stability of synaptic structures during synaptic plasticity. *Neuron*. 2014;82:430–443.
32. Desmond NL, Levy WB. Synaptic correlates of associative potentiation/depression: an ultrastructural study in the hippocampus. *Brain Res*. 1983;265:21–30.
33. Nägerl UV, Eberhorn N, Cambridge SB, Bonhoeffer T. Bidirectional activity-dependent morphological plasticity in hippocampal neurons. *Neuron*. 2004;44:759–767.
34. Zhou Q, Homma KJ, Poo MM. Shrinkage of dendritic spines associated with long-term depression of hippocampal synapses. *Neuron*. 2004;44:749–757.
35. Arellano JI, Benavides-Piccione R, Defelipe J, Yuste R. Ultrastructure of dendritic spines: correlation between synaptic and spine morphologies. *Front Neurosci*. 2007;1:131–143.
36. Meador-Woodruff JH, Hogg AJ Jr, Smith RE. Striatal ionotropic glutamate receptor expression in schizophrenia, bipolar disorder, and major depressive disorder. *Brain Res Bull*. 2001;55:631–640.
37. Gupta DS, McCullumsmith RE, Beneyto M, Haroutunian V, Davis KL, Meador-Woodruff JH. Metabotropic glutamate receptor protein expression in the prefrontal cortex and striatum in schizophrenia. *Synapse*. 2005;57:123–131.
38. Aparicio-Legarza MI, Davis B, Hutson PH, Reynolds GP. Increased density of glutamate/N-methyl-D-aspartate receptors in putamen from schizophrenic patients. *Neurosci Lett*. 1998;241:143–146.
39. Noga JT, Hyde TM, Herman MM, et al. Glutamate receptors in the postmortem striatum of schizophrenic, suicide, and control brains. *Synapse*. 1997;27:168–176.
40. Freed WJ, Dillon-Carter O, Kleinman JE. Properties of [3H] AMPA binding in postmortem human brain from psychotic subjects and controls: increases in caudate nucleus associated with suicide. *Exp Neurol*. 1993;121:48–56.
41. Healy DJ, Haroutunian V, Powchik P, et al. AMPA receptor binding and subunit mRNA expression in prefrontal cortex and striatum of elderly schizophrenics. *Neuropsychopharmacology*. 1998;19:278–286.
42. Kristiansen L, Meador-Woodruff J. Abnormal striatal expression of transcripts encoding NMDA interacting PSD proteins in schizophrenia, bipolar disorder and major depression. *Schizophr Res*. 2005;78:8793.
43. Forder JP, Tymianski M. Postsynaptic mechanisms of excitotoxicity: involvement of postsynaptic density proteins, radicals, and oxidant molecules. *Neuroscience*. 2009;158:293–300.
44. Pickel VM, Beckley SC, Joh TH, Reis DJ. Ultrastructural immunocytochemical localization of tyrosine hydroxylase in the neostriatum. *Brain Res*. 1981;225:373–385.
45. Somerville SM, Lahti AC, Conley RR, Roberts RC. Mitochondria in the striatum of subjects with schizophrenia: relationship to treatment response. *Synapse*. 2011;65:215–224.

46. Somerville SM, Conley RR, Roberts RC. Striatal mitochondria in subjects with chronic undifferentiated vs. chronic paranoid schizophrenia. *Synapse*. 2012;66:29–41.
47. Somerville SM, Conley RR, Roberts RC. Mitochondria in the striatum of subjects with schizophrenia. *World J Biol Psychiatry*. 2011;12:48–56.
48. Kung L, Roberts RC. Mitochondrial pathology in human schizophrenic striatum: a postmortem ultrastructural study. *Synapse*. 1999;31:67–75.
49. Mamdani F, Rollins B, Morgan L, Sequeira PA, Vawter MP. The somatic common deletion in mitochondrial DNA is decreased in schizophrenia. *Schizophr Res*. 2014;159:370–375.
50. Sequeira A, Martin MV, Rollins B, et al. Mitochondrial mutations and polymorphisms in psychiatric disorders. *Front Genet*. 2012;3:103.
51. Prince JA, Blennow K, Gottfries CG, Karlsson I, Oreland L. Mitochondrial function is differentially altered in the basal ganglia of chronic schizophrenics. *Neuropsychopharmacology*. 1999;21:372–379.
52. Prince JA, Harro J, Blennow K, Gottfries CG, Oreland L. Putamen mitochondrial energy metabolism is highly correlated to emotional and intellectual impairment in schizophrenics. *Neuropsychopharmacology*. 2000;22:284–292.
53. Groenewegen HJ, Wright CI, Beijer AV, Voorn P. Convergence and segregation of ventral striatal inputs and outputs. *Ann N Y Acad Sci*. 1999;877:49–63.
54. Haber SN, McFarland NR. The concept of the ventral striatum in nonhuman primates. *Ann N Y Acad Sci*. 1999;877:33–48.
55. Zahm DS. Functional-anatomical implications of the nucleus accumbens core and shell subterritories. *Ann N Y Acad Sci*. 1999;877:113–128.
56. Deutch AY, Lee MC, Iadarola MJ. Regionally specific effects of atypical antipsychotic drugs on striatal Fos expression: the nucleus accumbens shell as a locus of antipsychotic action. *Mol Cell Neurosci*. 1992;3:332–341.
57. Merchant K, Dorsa D. Differential induction of neurotensin and c-fos gene expression by typical versus atypical antipsychotics. *Proc Natl Acad Sci U S A*. 1993;90:3447–3451.
58. Robertson GS, Fibiger HC. Neuroleptics increase c-fos expression in the forebrain: contrasting effects of haloperidol and clozapine. *Neuroscience*. 1992;46:315–328.
59. Heimer L, Zahm DS, Churchill L, Kalivas PW, Wohltmann C. Specificity in the projection patterns of accumbal core and shell in the rat. *Neuroscience*. 1991;41:89–125.
60. Zahm DS, Brog JS. On the significance of subterritories in the "accumbens" part of the rat ventral striatum. *Neuroscience*. 1992;50:751–767.
61. Groenewegen HJ, Wright CI, Beijer AV. The nucleus accumbens: gateway for limbic structures to reach the motor system? *Prog Brain Res*. 1996;107:485–511.
62. Kuepper R, Skinbjerg M, Abi-Dargham A. The dopamine dysfunction in schizophrenia revisited: new insights into topography and course. *Handb Exp Pharmacol*. 2012:1–26.
63. Deutch AY, Cameron DS. Pharmacological characterization of dopamine systems in the nucleus accumbens core and shell. *Neuroscience*. 1992;46:49–56.
64. Howes OD, Montgomery AJ, Asselin MC, et al. Elevated striatal dopamine function linked to prodromal signs of schizophrenia. *Arch Gen Psychiatry*. 2009;66:13–20.
65. Kegeles LS, Abi-Dargham A, Frankle WG, et al. Increased synaptic dopamine function in associative regions of the striatum in schizophrenia. *Arch Gen Psychiatry*. 2010;67:231–239.
66. Lodge DJ, Grace AA. Hippocampal dysregulation of dopamine system function and the pathophysiology of schizophrenia. *Trends Pharmacol Sci*. 2011;32:507–513.
67. Lisman J. Excitation, inhibition, local oscillations, or large-scale loops: what causes the symptoms of schizophrenia? *Curr Opin Neurobiol*. 2012;22:537–544.
68. Boley AM, Perez SM, Lodge DJ. A fundamental role for hippocampal parvalbumin in the dopamine hyperfunction associated with schizophrenia. *Schizophr Res*. 2014;157:238–243.
69. Lodge D, Grace A. Aberrant hippocampal activity underlies the dopamine dysregulation in an animal model of schizophrenia. *J Neurosci*. 2007;27:11424–11430.
70. French S, Totterdell S. Quantification of morphological differences in boutons from different afferent populations to the nucleus accumbens. *Brain Res*. 2004;1007:167177.
71. Zhang ZJ, Reynolds GP. A selective decrease in the relative density of parvalbumin-immunoreactive neurons in the hippocampus in schizophrenia. *Schizophr Res*. 2002;55:1–10.
72. Knable MB, Barci BM, Webster MJ, Meador-Woodruff J, Torrey EF. Molecular abnormalities of the hippocampus in severe psychiatric illness: postmortem findings from the Stanley Neuropathology Consortium. *Mol Psychiatry*. 2004;9:609–620, 544.
73. Konradi C, Yang CK, Zimmerman EI, et al. Hippocampal interneurons are abnormal in schizophrenia. *Schizophr Res*. 2011;131:165–173.
74. Wang AY, Lohmann KM, Yang CK, et al. Bipolar disorder type 1 and schizophrenia are accompanied by decreased density of parvalbumin- and somatostatin-positive interneurons in the parahippocampal region. *Acta Neuropathol*. 2011;122:615–626.
75. Heckers S, Rauch SL, Goff D, et al. Impaired recruitment of the hippocampus during conscious recollection in schizophrenia. *Nat Neurosci*. 1998;1:318–323.
76. Medoff DR, Holcomb HH, Lahti AC, Tamminga CA. Probing the human hippocampus using rCBF: contrasts in schizophrenia. *Hippocampus*. 2001;11:543–550.
77. Kelley AE, Domesick VB. The distribution of the projection from the hippocampal formation to the nucleus accumbens in the rat: an anterograde- and retrograde-horseradish peroxidase study. *Neuroscience*. 1982;7:2321–2335.
78. Groenewegen H, Zee E, Kortschot A, Witter M. Organization of the projections from the subiculum to the ventral striatum in the rat. A study using anterograde transport of *Phaseolus vulgaris* leucoagglutinin. *Neuroscience*. 1987;23:103–120.
79. Blaha CD, Yang CR, Floresco SB, Barr AM, Phillips AG. Stimulation of the ventral subiculum of the hippocampus evokes glutamate receptor-mediated changes in dopamine efflux in the rat nucleus accumbens. *Eur J Neurosci*. 1997;9:902–911.
80. Brudzynski SM, Gibson CJ. Release of dopamine in the nucleus accumbens caused by stimulation of the subiculum in freely moving rats. *Brain Res Bull*. 1997;42:303–308.
81. Floresco SB, Todd CL, Grace AA. Glutamatergic afferents from the hippocampus to the nucleus accumbens regulate activity of ventral tegmental area dopamine neurons. *J Neurosci*. 2001;21:4915–4922.
82. O'Donnell P, Greene J, Pabello N, Lewis BL, Grace AA. Modulation of cell firing in the nucleus accumbens. *Ann N Y Acad Sci*. 1999;877:157–175.
83. Knutson B, Bjork JM, Fong GW, Hommer D, Mattay VS, Weinberger DR. Amphetamine modulates human incentive processing. *Neuron*. 2004;43:261–269.

84. Juckel G, Schlagenhauf F, Koslowski M, et al. Dysfunction of ventral striatal reward prediction in schizophrenia. *Neuroimage*. 2006;29:409–416.
85. Roberts RC, Gaither LA, Gao XM, Kashyap SM, Tamminga CA. Ultrastructural correlates of haloperidol-induced oral dyskinesias in rat striatum. *Synapse*. 1995;20:234–243.
86. Meshul CK, Andreassen OA, Allen C, Jørgensen HA. Correlation of vacuous chewing movements with morphological changes in rats following 1-year treatment with haloperidol. *Psychopharmacology (Berl)*. 1996;125:238–247.
87. Kelley J, Gao X, Tamminga C, Roberts R. The effect of chronic haloperidol treatment on dendritic spines in the rat striatum. *Exp Neurol*. 1997;146:471–478.
88. Meshul CK, Casey DE. Regional, reversible ultrastructural changes in rat brain with chronic neuroleptic treatment. *Brain Res*. 1989;489:338–346.
89. Meshul CK, Janowsky A, Casey DE, Stallbaumer RK, Taylor B. Effect of haloperidol and clozapine on the density of "perforated" synapses in caudate, nucleus accumbens, and medial prefrontal cortex. *Psychopharmacology (Berl)*. 1992;106:45–52.
90. See RE, Chapman MA, Meshul CK. Comparison of chronic intermittent haloperidol and raclopride effects on striatal dopamine release and synaptic ultrastructure in rats. *Synapse*. 1992;12:147–154.
91. Chakos MH, Lieberman JA, Alvir J, Bilder R, Ashtari M. Caudate nuclei volumes in schizophrenic patients treated with typical antipsychotics or clozapine. *Lancet*. 1995;345: 456–457.
92. Chakos MH, Lieberman JA, Bilder RM, et al. Increase in caudate nuclei volumes of first-episode schizophrenic patients taking antipsychotic drugs. *Am J Psychiatry*. 1994;151:1430–1436.
93. Chakos MH, Shirakawa O, Lieberman J, Lee H, Bilder R, Tamminga CA. Striatal enlargement in rats chronically treated with neuroleptic. *Biol Psychiatry*. 1998;44:675–684.
94. Corson PW, Nopoulos P, Miller DD, Arndt S, Andreasen NC. Change in basal ganglia volume over 2 years in patients with schizophrenia: typical versus atypical neuroleptics. *Am J Psychiatry*. 1999;156:1200–1204.
95. Keshavan MS, Bagwell WW, Haas GL, Sweeney JA, Schooler NR, Pettegrew JW. Changes in caudate volume with neuroleptic treatment. *Lancet*. 1994;344:1434.
96. Heimer L, Alheid GF, de Olmos JS, et al. The accumbens: beyond the core-shell dichotomy. *J Neuropsychiatry Clin Neurosci*. 1997;9:354–381.
97. Ikemoto K, Satoh K, Maeda T, Fibiger HC. Neurochemical heterogeneity of the primate nucleus accumbens. *Exp Brain Res*. 1995;104:177–190.
98. Meredith GE, Pattiselanno A, Groenewegen HJ, Haber SN. Shell and core in monkey and human nucleus accumbens identified with antibodies to calbindin-D28k. *J Comp Neurol*. 1996;365:628–639.